Mechanical Failure Modes and Longevity of Geomembranes – 16365

Kevin Foye, Ph.D.*, P.E., Te-Yang Soong, Ph.D., P.E.*
*CTI and Associates, Inc., 51331 W. Pontiac Trail, Wixom, MI 48393 USA
(*kfoye@cticompanies.com, tsoong@cticompanies.com)*

ABSTRACT

Estimates of the long-term performance of geosynthetic liner and final cover components have traditionally relied on a small number of standard assumptions originally developed to address the needs of the Resource Conservation and Recovery Act (RCRA) Subtitle D solid waste industry. These past estimates demonstrated that, even under a series of highly conservative factors, the longevity of these components far exceeds the requirements for typical municipal solid waste (MSW) facilities. However, interest in the performance of these components for the disposal of low-level (LLW) and intermediate-level (ILW) radioactive waste landfills has led to additional study of geosynthetic degradation to address longer assessment periods. These studies allow for the possibility of more rigorous, reliability-based risk assessments of landfill system performance. A particularly strong research need for LLW/ILW facilities is a complete enumeration of the various chemical and mechanical failures modes for geomembranes serving as final cover and base liner barrier systems. For final covers, failure is defined as allowing an unacceptable flow of water into a containment system. Studies of the various mechanical modes of deformation and rupture for polyethylene sheet allow for a rigorous exploration of the potential causes of geomembrane barrier system failure. Of particular interest in the performance assessment and engineering of these systems is the ability to use the resulting models to quantify the longevity of these systems with a probabilistic model. An example of this approach is used to illustrate how the consideration of the mechanism for stress cracking in final cover geomembranes can be adapted for use in simulations of long-term landfill system performance. The results indicate that the effects of cover system design geometry and geomembrane formulation on performance can be varied significantly by the cover system engineering to meet target performance goals.

INTRODUCTION

Geomembranes are a key component of landfill final cover systems, acting as a barrier to water infiltration into landfills. Figure 1 presents a cross-section view of the typical components of a composite final cover system incorporating a geomembrane. Other common geosynthetic components of a typical final cover include, a geotextile/geonet geocomposite drainage layer in place of the granular drainage media, and a geocomposite clay liner to augment the geomembrane and/or substitute or supplement the clay barrier. Other cover components shown in Figure 1 include the topsoil layer, which resists erosion and facilitates vegetative growth; protective soil, which acts as a further buffer to erosion, animal intrusion, root growth, and frost intrusion; and the barrier clay, which acts together with the geomembrane as a composite barrier to surface water infiltration.

Water is introduced to the cover system in the form of atmospheric precipitation onto the cover surface. Some of this water does not enter the soil and is drained as run-off water. Other water is stored in the topsoil, taken up by plants, and returned to the atmosphere via evapotranspiration. The remaining water percolates vertically to the drainage media, where it is intercepted by the composite barrier and diverted to drainage structures. A smaller fraction of the percolated water may enter the barrier clay through holes in the geomembrane or via diffusion through the geomembrane. Water that enters the barrier clay can then percolate through the barrier clay and eventually enter the landfill below.

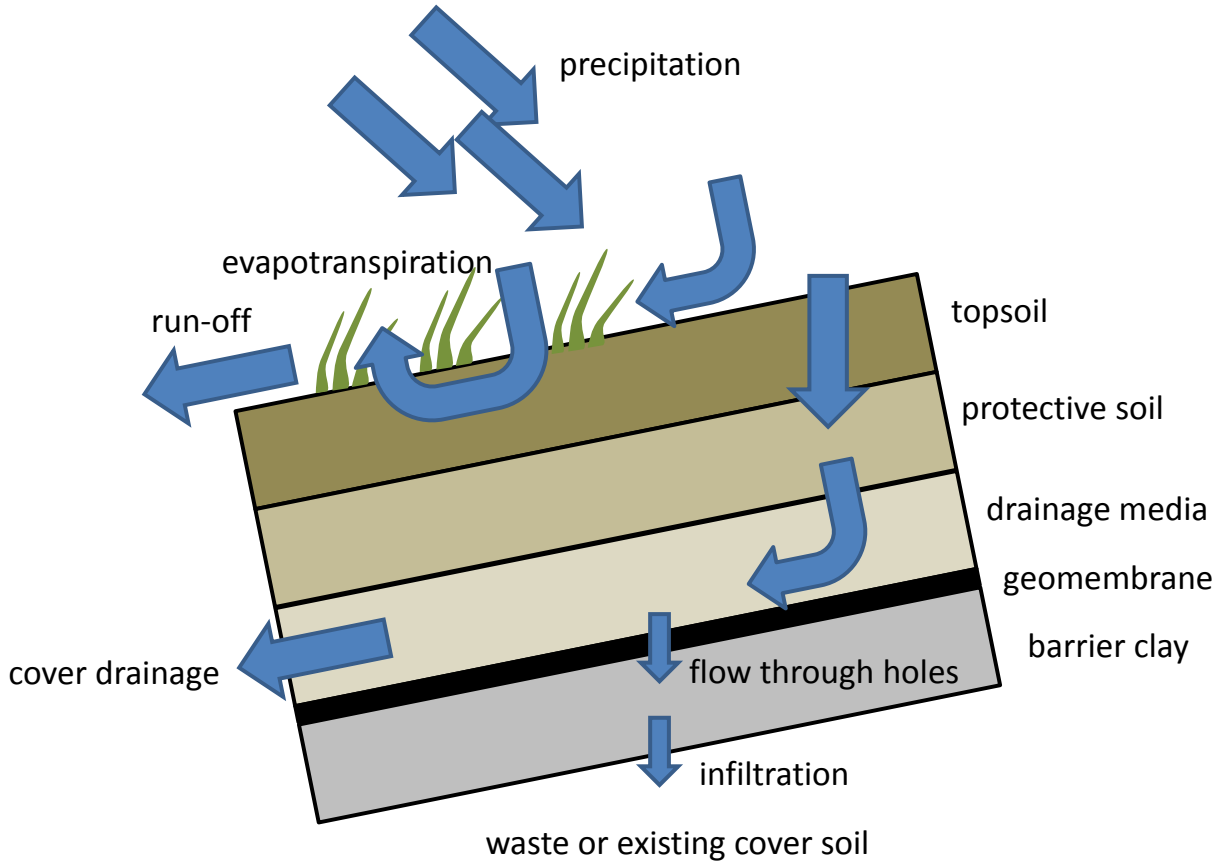

Figure 1. Typical Cover System Configuration Incorporating Geosynthetics

Equations to describe the flow of water through geomebrane holes into the underlying clay barrier have been proposed by several authors, for example [1] [2] [3] [4]. These equations are very important for the performance assessment of landfills because they describe the potential flow rate of water through the final cover into the landfill, a process that can result in the transport of contaminants from the landfill. In the absence of holes, the geomembrane functions as an effective barrier to this flow. Accordingly, several studies have investigated the long-term durability of geomembranes, for example [5] [6] [7] [8] [9] [10] [11] [12]. These studies consider the effects of chemical changes over time in the polymers comprising the geomembrane and the resulting changes in the mechanical properties of the geomembrane. This body of knowledge, while critical to understanding the

engineering behavior of these materials, does not directly describe how these processes and properties affect the formation of holes through which water could flow through final cover systems.

Therefore, an investigation of the mechanisms by which geomembranes develop holes is needed. Holes in final cover geomembranes can have the following causes: manufacturing, transportation, and handling damage/defects [13] [14], installation defects [4], post-installation disturbance (people, animals, plant roots) [9] [14], and stress cracks [9] [13]. Damage and defects that occur prior to the completion of construction of final cover systems are routinely addressed through inspection and testing programs [13] [14]. Disturbance from plants and animals is limited to very low levels by the physical configuration of the topsoil and protective soil (Figure 1). These measures are regarded as thoroughly effective [9]. Disturbance from people is difficult to model and is often addressed through intruder barriers. Intruders typically affect multiple landfill components, not only the final cover [15]. Stress cracks are a significant potential source of holes and are an on-going subject of research in the plastic pipe and geomembrane fields (e.g., [16] [17]). Existing materials tests and experiments focus on either directly observing the development of cracks under conditions replicating the in-service environment (e.g., [18]) or on generating repeatable index test results indicative of desirable stress crack resistance properties (e.g., [19] [20]). Based on this review, stress cracks appear to be the most relevant mechanism for the development of holes in final cover geomembranes. Stress cracking is therefore investigated as a potential source of holes and a framework for the quantification of this effect is presented.

STRESS CRACKING IN POLYETHYLENE

Most geomembranes used for final cover systems are manufactured from polyethylene (PE), a type of polymer. A common formulation of polyethylene used in environmental applications is identified as High-Density Polyethylene (HDPE). A relatively large body of research into the properties of HDPE is available. In order to understand the mechanical properties of polyethylene relevant to cracking in final covers, a discussion of the micromechanics of PE is required.

Similar to other polymers, PE materials are an assemblage of long, chain-like molecules synthesized by the polymerization of ethylene. Different polymerization techniques result in varying molecule lengths and branching structures. The molecule lengths are principally measured in terms of molecular weight. The branching structure of PE is able to be indirectly determined by measuring the density of the material in aggregate for the following reasons. PE is a semi-crystalline material, meaning it has regions of closely-packed chains with regularly-oriented directions and relatively strong inter-molecular forces and also regions of more random, looser configured chains. These arrangements are illustrated in Figure 2. Due to the appearance of the structure of the molecule assemblages, the crystalline regions are known as lamellae while the zones in between are known as amorphous regions. More closely arranged molecules result in a higher proportion of lamellae and therefore greater density. PE molecules with large or multiple branches cannot

become closely aligned. Therefore, PE formulations with fewer and shorter branches exhibit greater crystallinity and greater density. Conversely, more branches and longer branches result in lower density PE formulations [18].

The arrangement of the PE molecules is directly responsible for the mechanical behavior of the material in aggregate. Similarly to other materials, studies of the mechanical behavior of PE often focus on tests of the response of the material to the application of tensile forces in varying intensity and duration. The response of PE to forces is described as visco-elastic, meaning that the development of strains in response to applied stresses is dependent on time. For example, as illustrated in Figure 2, the progression from the initial structure to the relatively short-duration ductile failure mode involves the stretching of the tie molecules between lamellae and the breakup of the lamellae into smaller units which can then displace. In contrast, the relatively long-duration brittle failure mode involves the gradual disentanglement of the tie molecules which culminates in the separation of the lamellae that were once tied together [17]. This mode of failure is responsible for stress cracking, which is defined at the rupture of PE under stresses less than the short term strength [20]. Cracking specifically develops in response to locally intensified loading, often caused by scratches, gouges, or abrupt changes in geometry [18]. The longer-term displacement of molecules can also appear as creep (deformation under constant load) or stress relaxation (reduction in stress at a fixed deformation) in PE specimens loaded over long periods of time.

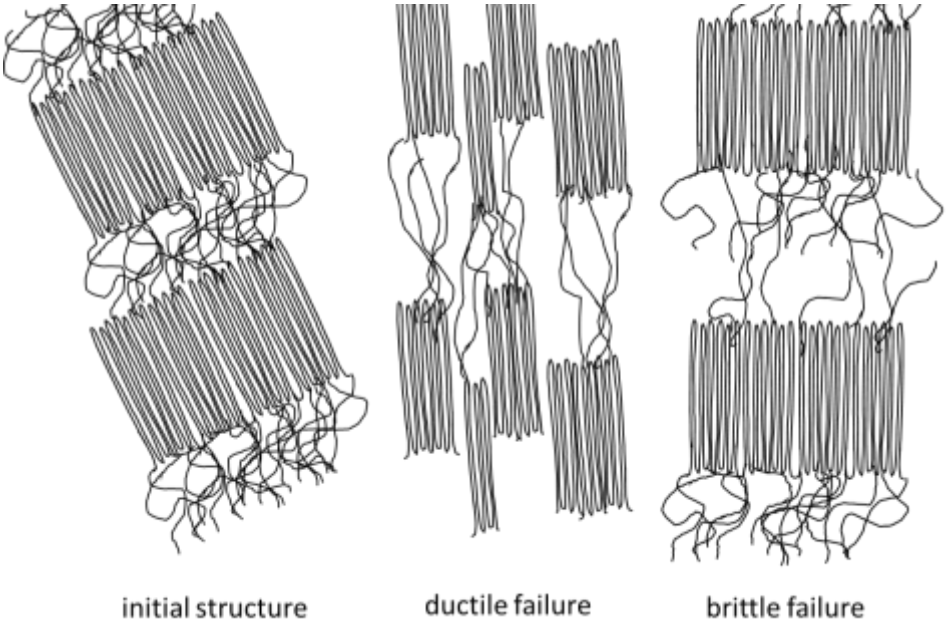

Figure 2. Illustration of the Structure of Polyethylene Molecules and Mechanisms of Failure (adapted from [17] [20] [21])

Table I summarizes the implications of this molecular-level understanding of PE mechanics for the properties of PE required for final cover design. Of particular note in Table I is the inherent conflict between different properties considered beneficial to PE geomembrane performance. Higher density and greater crystallinity results in

greater chemical resistance, which is good for geomembrane durability. However, higher density and greater crystallinity also result in more stress crack susceptibility [17] [18]. Therefore, skillful engineering of PE geomembranes should involve the balancing of properties to meet the performance objectives.

TABLE I. Selected Mechanical Properties of Polyethylene and Implications for Selecting Density

Mechanical Property Name	**Significance for Polyethylene Mechanics**	**Effect of Increasing Density**
Tensile Strength at Yield	Stronger material (more tightly organized molecules) can resist larger loads before permanent deformation	Increases
Stiffness	Stiffer material deforms less under stress	Increases
Impact Strength	Large, short duration stresses can cause rapid crack development. Robust tie molecule networks can reduce vulnerability to cracking.	Decreases
Stress Crack Resistance	Long-duration loads significantly less than yield can, over time, result in disentanglement of tie molecules and separation of lamellae. Broad distributions of tie molecules with multiple interlocking branches resist cracking.	Decreases
Permeability	More tightly organized molecules admit fewer outside molecules through the matrix.	Decreases
Chemical Resistance	More tightly organized molecules are less available to react with outside molecules.	Increases

In addition to density, other properties that contribute to stress crack resistance are molecular weight and molecular weight distribution [18]. As the PE chains become longer and more varied, they are better able to resist the disentanglement that results in the development of the brittle failure mode [17]. Numerous tests are available to the polymer industry to measure these properties. Accordingly, PE formulations can be ordered specifically to provide the desired properties, as has been illustrated by developments in PE pipe formulations [18].

STRESS CRACKING IN POLYETHYLENE GEOMEMBRANES

The next issue to be addressed is whether or not final cover geomembranes are likely to have the conditions required for stress cracking to occur. In principle, because of the geometry of the final cover system shown in Figure 1 and because the

geosynthetic and soil layers are typically selected such that all sliding forces are balanced by frictional interface properties, there should be no development of tensile stresses within the geomembrane layer. This concept of the stress state of installed geomembranes is illustrated in Figure 3. As shown in Figure 3, the overburden stress above the uniform PE geomembrane sheet is balanced by the subgrade reaction. Any attempt to deform laterally is constrained by the presence of adjacent materials. Furthermore, the Poisson's ratio of PE is 0.45 [18], a value very close to 0.5, where there is no volume change under loading. Therefore, in the case of a geomembrane within a final cover system, due to the nearly uniform overburden pressure, combined with lateral confinement resulting from large areal extent of installation, little reduction in thickness is expected with time. The resulting state of stress for the PE geomembrane is represented by the Mohr's circle of stresses shown in Figure 4(a). In this figure, normal stresses (σ) are plotted on the horizontal axis and shear stresses (τ) are plotted on the vertical axis. The major and minor principal stresses are denoted σ_1 and σ_2, respectively. Figure 4(a) illustrates that under Figure 3 conditions, all stresses within the geomebrane are compressive. This state of stress for installed geomembranes has been theorized by others, notably [9].

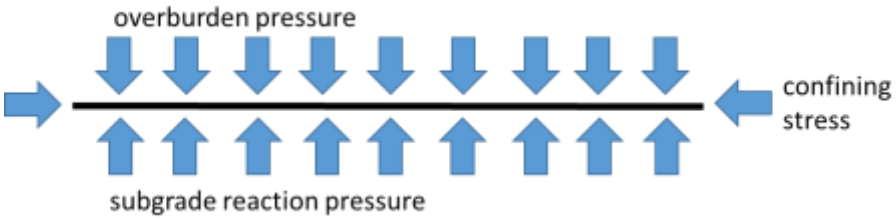

Figure 3. Idealization of Forces Acting on Final Cover Polyethylene Geomembrane Cross-Section.

The shortcoming of the theory illustrated in Figure 3 is that installed PE geomembranes actually contain significant numbers of discontinuities that need to be considered with regards to their potential to initiate stress cracking. Specifically, even for flawlessly installed geomembrane layers, multiple geomembrane panels of finite width must be seamed together. The current preferred state-of-the-art method for joining PE gemembrane panels in the field in thermo-fusion welding, also known as hot wedge seaming, for which exacting specifications are available to produce high-quality seams [22]. Figure 5 depicts a PE geomebrane installation in progress wherein panels have been joined by thermo-fusion methods. The geomembrane panels shown in Figure 5 are 7 m wide and have been joined by "double-wedge weld" technique, which creates a central air channel within the seam that can be subsequently pressure tested to evaluate the continuity of the seam. Figure 6 depicts a typical double-wedge welded seam cross section with visible air channel. Figure 7 depicts a similar cross section through an extrusion-welded seam. Extrusion welding is a less-preferred method of seaming wherein a molten bead of PE is extruded along overlapping geomembrane edges in order to weld them together. Extrusion welding is often used to seam PE geomembrane panels in places where thermo-fusion equipment will not fit.

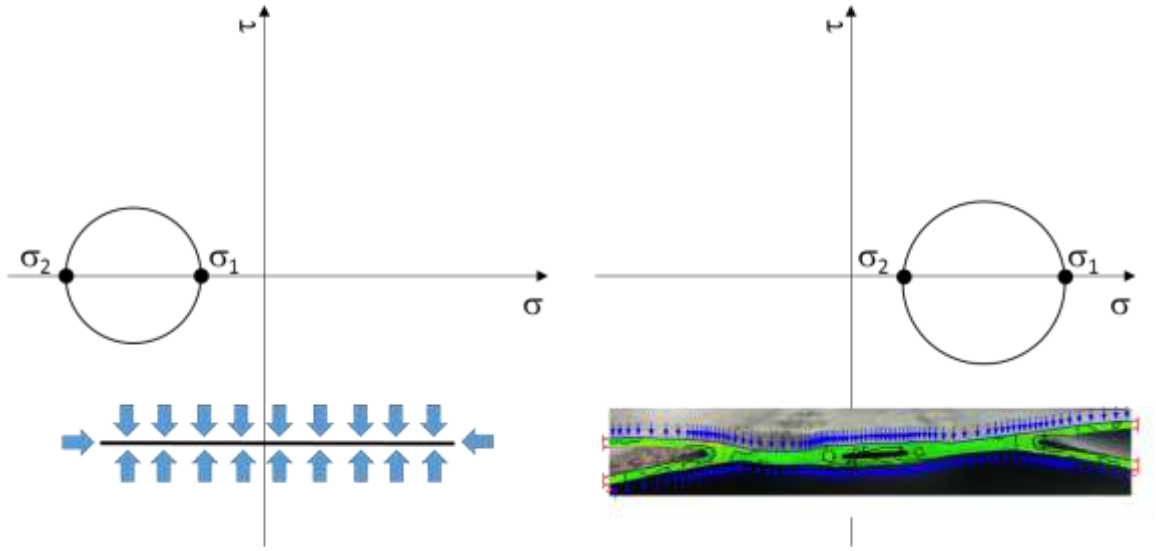

(a) (b)

Figure 4. Example Mohr's Circles of Stresses. (a) Confined, Uniform Section; (b) Maximum Tensile Stress at Extreme Fiber from a Thermo-Fusion Seam Section

Figure 5. Photo of Typical Geomembrane Installation in Progress. Note Relative Panel Width and Seam Locations.

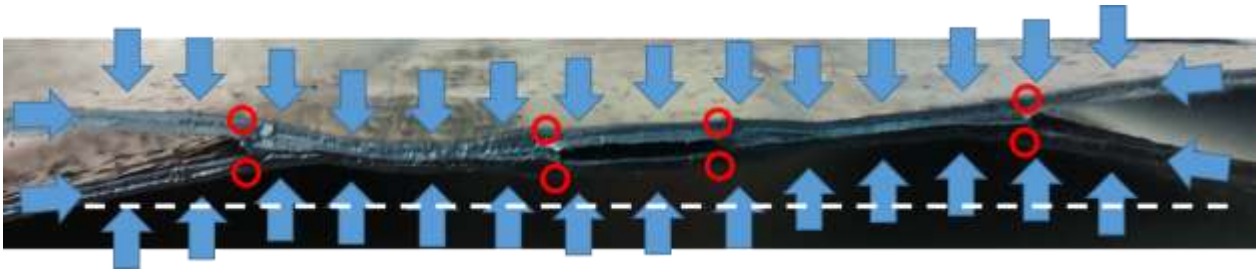

Figure 6. Diagram of Final Cover Forces Acting on Geomembrane Fusion Seam Cross-Section. Red Circles Indicate Locations of Expected Tensile Stress Concentration.

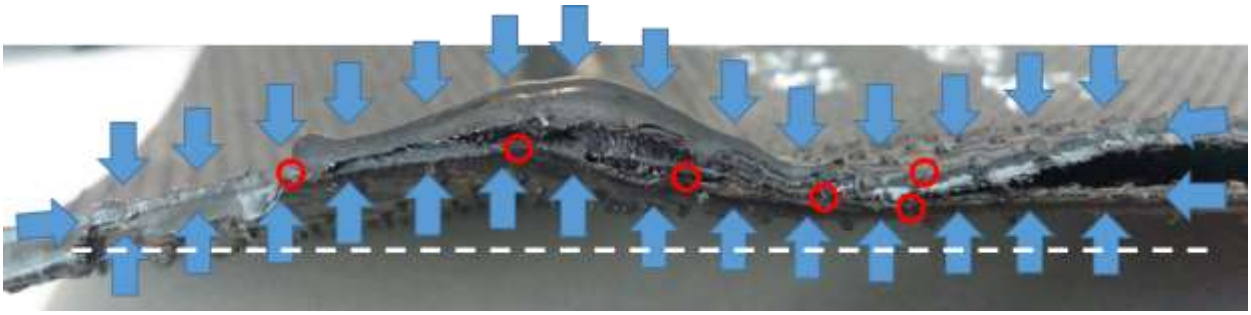

Figure 7. Diagram of Final Cover Forces Acting on Geomembrane Extrusion Seam Cross-Section. Red Circles Indicate Locations of Expected Tensile Stress Concentration.

Similar to Figure 3, Figures 6 and 7 also have arrows illustrating the action of forces on the cross section. Considering that the samples depicted in Figures 6 and 7 were not loaded at the time they were photographed, their shapes represent a relatively stress-neutral state, with only the forces locked-in by welding and thermal deformation present. The white dashed line in Figures 6 and 7 suggests the shape of the flat subgrade to which the geomebrane will be forced to conform under the action of the overburden stresses. Therefore, Figures 6 and 7 also have red circles highlighting portions of the cross section where the loading and subsequent deformation is expected to cause the generation of concentrated tensile stresses. In addition to these stress concentrations, the melting and straining of PE during welding modifies the structure of the PE locally, increasing the potential for cracking [18]. Finally, the presence of tool marks, weld beads, or scrapes in these locations can serve as the initiation point for crack propagation [20]. Therefore, geomebrane seams appear to be a potential location for the formation of stress cracks.

Because different PE formulations can exhibit different degrees of susceptibility to stress cracking, quantitative methods are needed to describe this behavior. The measurement of stress crack resistance in geomembranes is accomplished using a standardized test known as the Notched Constant Tensile Load (NCTL) test [19] [20]. During the test, multiple dumbbell-shaped specimens are cut to standard dimensions and scored to a depth 20% of the geomembrane thickness at their center. This scored notch becomes the initiation point for stress cracking during the test. Each sample is subjected to contact tensile load. The tensile loads are reported in terms of their ratio to the tensile strength at yield (σ_y):

$$\psi = \frac{\sigma}{\sigma_y} \quad \text{(Eq. 1)}$$

where σ is the applied stress during the test. Under the action of the constant load, the time until the specimen ruptures is recorded as the time to failure t_f. Figure 8 represents the resulting plot of failure stress ratios ψ_f versus times to failure t_f. One notable feature of Figure 8 is the transition between the ductile and brittle failure modes represented by the change in slope of the test results. This point is called the transition point. The transition time t_t and transition stress ψ_t are reported results of the NCTL test. The slope s of each curve in log-log scale is also reported. With regards to stress cracking, the brittle failure line is of particular interest. The equation of this line can be written

$$t_f = \left(\frac{t_t}{\psi_t^{s^{-1}}}\right)\psi_f^{s^{-1}} \quad \text{(Eq. 2)}$$

Because it takes a long time for stress cracks to develop in PE geomebranes during the NCTL test, the test is typically run at elevated temperatures, such as 50ºC. While useful in developing a standard index measure for the relative quality of PE samples, this temperature is not representative of in-service conditions for final cover geomebranes. A temperature of 20ºC is more representative. Therefore, in order to attempt a quantification of the stress crack effect on final cover system performance, an estimate of the brittle failure line at 20ºC is needed. For the engineering and performance assessment of specific final cover systems, engineers should perform NCTL tests on the actual PE geomembrane formulations being considered for the project. For the purposes of this example, published values provided by [20] are used. It is also important to note that standard NCTL tests are performed with the test samples immersed in a surfactant solution, which, through its action on the PE chains, further accelerates the cracking effect. Therefore, the use of these results in evaluations of final cover geomebrane performance is considered especially conservative since actual in-service conditions are not expected to be as chemically hostile to PE.

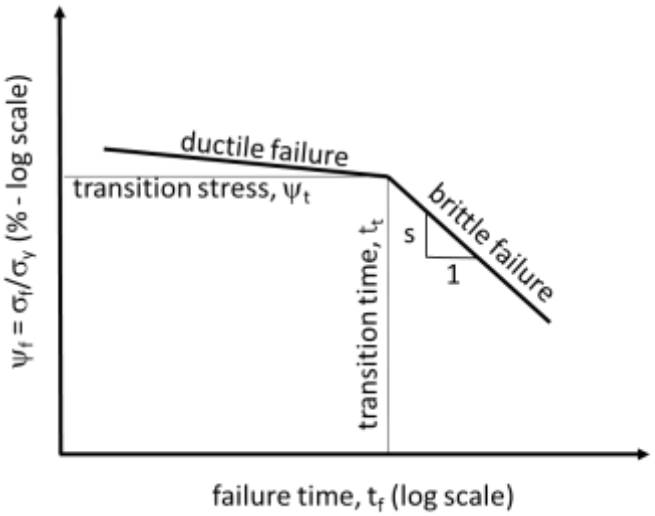

Figure 8. Interpretation of the Results of a Notched Constant Tensile Load (NCTL) Test Series.

NCTL test results reported by [20] are given for samples evaluated at 40ºC and 50ºC. These results for ψ_f versus t_f can be used to interpret the corresponding values at 20ºC using rate process theory [18] [20]:

$$\log(t_f) = A_0 + \frac{A_1}{T} + \frac{A_2}{T}\log(\psi_f) \quad \text{(Eq. 3)}$$

Where T is the test temperature in Kelvin and A_0, A_1, and A_2 are constants determined through calibration to the 40ºC and 50ºC results. For the experimental data collected by [20] from the NCTL testing of HDPE geomembrane samples, the resulting constants for the brittle failure line are -16.35, 6908, and -831.6, respectively. In terms of Eq. 2, these values yield s = -0.352, t_t = 144 hrs, and ψ_t = 60.58% for 20ºC. Acknowledging that the NCTL test is intended as an index test of stress crack resistance, it is still useful to consider its implications for the long-term performance of PE geomembrane seams in a final cover system. The following example provides a framework for the quantitative evaluation of seam lifetime using the results of the NCTL test.

FINAL COVER SEAM LIFE FOR PERFORMANCE ASSESSMENT

In order for the knowledge presented in the previous sections to be applied to the engineering and performance assessment of PE final cover geomembranes, the time to failure and its uncertainty must be calculated with respect to in-service stress states representative of final cover system. The following example presents a procedure to perform this calculation.

It is expected that the vertical overburden forces acting on the geomebrane seam cross section shown in Figure 6 will result in relatively large local tensile stresses concentrated at the extreme fiber of portions of the cross section undergoing flexure. These stress concentrations can be estimated through finite element analysis (FEA). Figure 9 shows a contour map of the maximum principal stresses (σ_1) obtained from FEA of the cross section from Figure 6. A uniform vertical pressure σ_v = 18 kPa was applied to the top and bottom surfaces, corresponding to a cover soil thickness of about 1 m. The red and yellow colors on the map indicate regions of greatest tensile stress. The area of greatest tensile stress in Figure 9 is just above and to the left of the left fusion welder track. In this location, FEA estimated σ_1 = 1,637 kPa and σ_2 = 98 kPa (see Figure 4b). The region below and to the right of the right track had calculated values σ_1 = 775 kPa and σ_2 = -2 kPa. These two sets of stress values are an estimate of possible stress concentration resulting from the seam discontinuities. A stress concentration factor, k, can be calculated as

$$k = \frac{\sigma_1}{\sigma_v} \quad \text{(Eq. 4)}$$

For the two locations identified, the resulting values of k are 90 and 43, respectively. Based on these results, the distribution of k is conservatively taken as a uniform distribution with bounds 150 and 50. This distribution is interpreted to represent the uncertainty in achieving particular values of stress concentration along the length of

the seam. Therefore, this distribution is related to the anticipated spatial distribution of stress cracking.

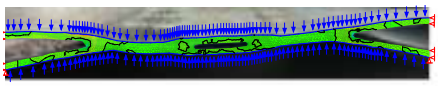

Figure 9. Contour Map of Maximum Principal Stresses (σ_1) within Geomembrane Fusion Seam Cross-Section from Finite Element Analysis. Red-Yellow Zones Indicate Locations of Tensile Stress Concentration.

In order to compare these stresses to the NCTL test results, stress ratio ψ must be calculated. Combining Eq. 1 and Eq. 4, the stress ratio can be calculated

$$\psi = \frac{k\sigma_v}{\sigma_y} = \frac{\sigma_1}{\sigma_y} \qquad \text{(Eq. 5)}$$

However, the stress in this cross section will not be constant with time due to stress relaxation in the PE. The stress $\sigma_{1,t}$ at time t is computed according to the following equation:

$$log(\sigma_{1,t}) = r[log(t) - log(t_0)] + \log(\sigma_{1,0}) \qquad \text{(Eq. 6)}$$

Where r is the slope of the empirical stress relaxation curves, t_0 is the time after loading for an initial modulus measurement, and $\sigma_{1,0}$ is the stress at time t_0. Empirical stress relaxation curves for PE are presented by [18] in terms of reduction in apparent modulus with time. These curves yield a nearly uniform value of r = -0.074 when t is in units of years.

Additionally, values of σ_y are not constant with time due to PE degradation from oxidation. The oxidation of PE follows the three-period process illustrated in Figure 10. During the antioxidant depletion and induction periods, no changes in the mechanical properties of PE are measured. Following the induction period, the oxidation of PE results in a decrease in mechanical properties according to a first-order decay process. A more thorough discussion of this process and its implications to geomembrane longevity is given by [23]. From a study of HDPE degradation by [8], the following equation was developed to quantify the degradation of σ_y:

$$\sigma_{y_t} = \begin{cases} \sigma_{y_0} & ,t \le t_A + t_B \\ \sigma_{y_0} e^{-\lambda(t - t_A - t_B)} & ,t > t_A + t_B \end{cases} \qquad \text{(Eq. 7)}$$

where σ_{yt} is the tensile strength at yield at time t, σ_{y0} is the initial tensile strength at yield, t_A is the length of the antioxidant depletion period, t_B is the length of the induction period, and λ is the decay constant. The study by [8] report the following values for an HDPE ageing experiment conducted at 20ºC: t_A = 208 years, t_B = 30 years, and λ = 0.003331 year^{-1}.

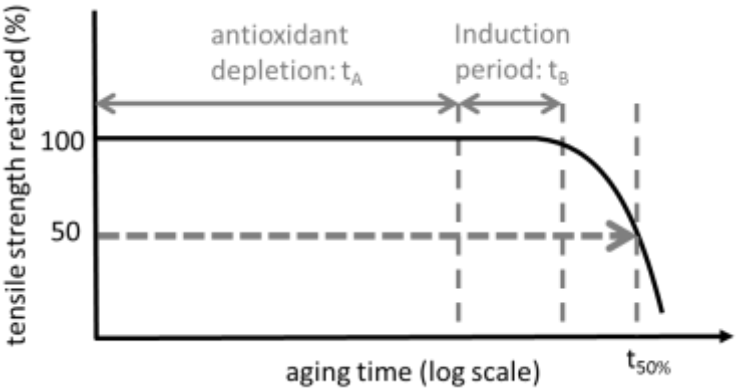

Figure 10. Degradation of Polyethylene Tensile Strength due to Oxidation (adapted from [8]).

Combining Equations 5, 6, and 7 results in a mean function with time for $\psi(\%)$ that can be conceptualized as the load demand on the PE geomembrane. This function represents estimated concentrated stress σ_1 and accounts for stress relaxation and material degradation. Figure 11 plots the resulting function, labeled "mean σ_1 est". A noteworthy feature of the σ_1 curve in Figure 11 is the pronounced inflection point after 238 years. This point represents the end of the induction period and the start of oxidation degradation of the tensile strength. Also plotted in Figure 11 is the mean brittle failure line from the NCTL tests, labeled "mean ψ_f". For clarity, the equation of this line is rearranged from Eq. 2 as follows:

$$log(\psi_f) = s\left[log(t_f) - log(t_t)\right] + \log(\psi_t) \qquad \text{(Eq. 8)}$$

The intersection of the σ_1 and stress crack load curves represents the mean estimate of the time required for stress cracks to develop in the HDPE seam. In this example, the mean time is about 240 years.

At this point, some limitations of these calculations must be discussed. First, applying NCTL test results to this problem ignores some important differences between the mechanics of the NCTL test and the PE geomembrane seam, such as the fact that σ_1 does not act across the entire geomembrane cross section as it does in the NCTL test. This approach would appear to be conservative. Second, the NCTL tests [20] and ageing tests [8] were performed under more chemically aggressive conditions than are anticipated for the final cover geomembrane. This condition is also conservative. Third, the test results used are from non-site specific HDPE formulations. It is possible for engineers to specify linear low-density PE (LLDPE) geomembranes with better stress crack performance than the HDPE results used in this example. Finally, the superposition of the two curves in Figure 11 as a method of analysis ignores the visco-elastic second-order effects taking place over time due to stress relaxation, ageing, polymer chain rearrangement, and crack development. In order to successfully model these results, a more comprehensive constitutive model is needed, perhaps similar to those proposed by [21] [24] [25] [26]. These models are

based on recent investigations into the mechanical behavior of PE at the microscopic and molecular level, quantifying the mechanisms illustrated in Figure 2.

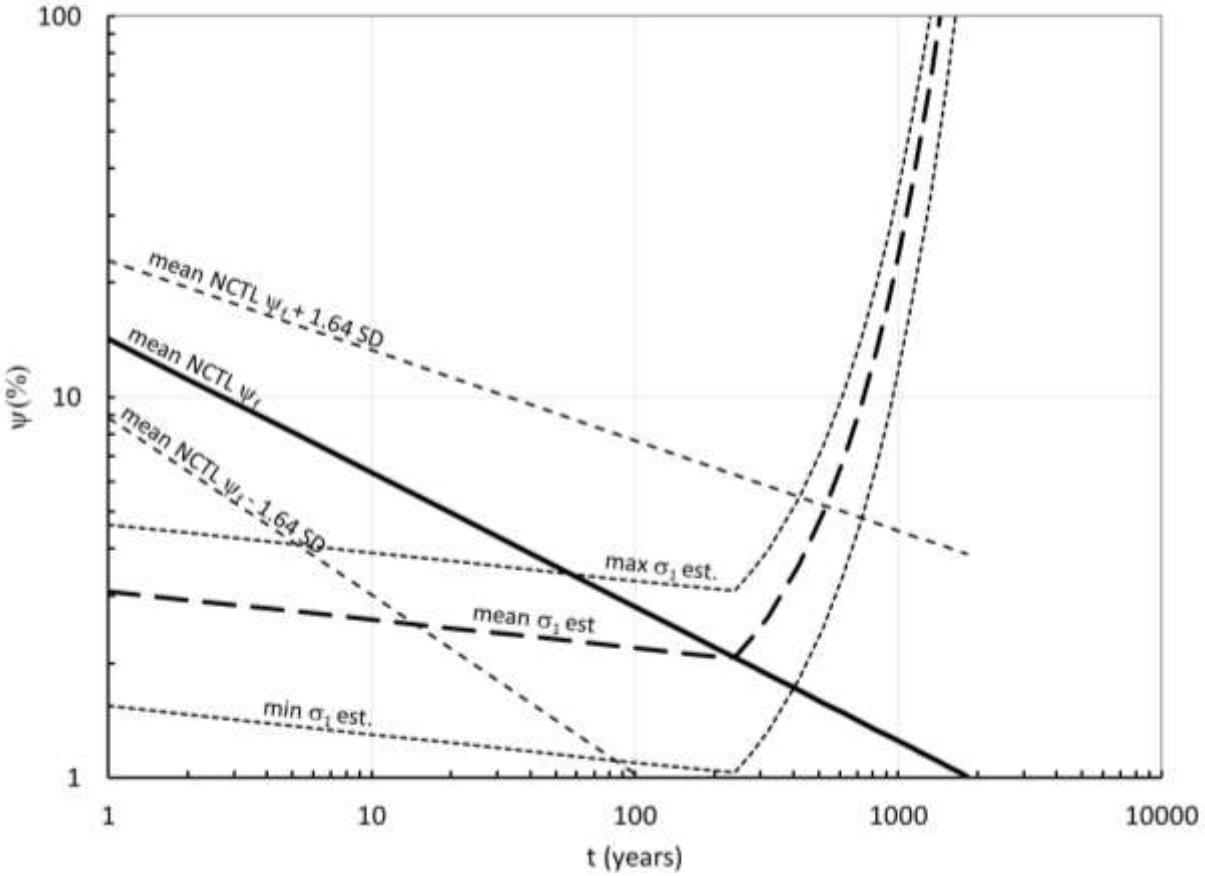

Figure 11. Comparison of Notched Constant Tensile Load (NCTL) at Failure (ψ_f) with Estimated Concentrated Maximum Tensile Stress (σ_1) Over Time.

In order to illustrate how this methodology can interface with performance assessments, which are interested both in modeling water flow into the landfill and accounting for the uncertainty in the model [6][15], two additional calculations are presented: generation of probability functions and estimation of leakage rate.

To consider the effect of uncertainty on estimates of PE geomebrane seam life, two additional sets of curves are plotted in Figure 11. The "max σ_1 est" and "min σ_1 est" curves correspond to k = 150 and k =50, respectively. These values were set as the limits on a uniform distribution for k based on the interpretation of the FEA results presented in Figure 9. The +1.64 SD and -1.64 SD stress crack load curves represent the 90% confidence limits on the stress crack load, calculated by varying the value of s according to uncertainty in the data obtained by [20]. A typical 20% coefficient of variation (COV) is observed for values of s determined from the cited NCTL test program. The significant differences in the time to failure between these curves illustrates the strong sensitivity of t_f estimates to these parameters.

Considering that performance assessments often consider stochastic landfill hydrology model at various "snapshots" in time, it is useful to generate Cumulative Distribution Functions (CDFs) for estimates of NCTL ψ_f and concentrated stress σ_1 for a specific time. Figure 12 plots the CDFs of these estimates for t = 100 years. To generate each of these CDFs, the Probability Density Function (PDF) for each equation was first transformed from the PDF for the input random variable X to the output random variable Y using the following equation [27]:

$$p_Y(y)dy = p_X[f^{-1}(y)]df^{-1}(y) \quad \text{(Eq. 9)}$$

where $p_Y(y)$ is the PDF of random variable Y, $p_X(x)$ is the PDF of random variable X, and $f^{-1}(y)$ is the inverse function of y = f(x). For this example, Eq. 9 was evaluated according to the methodology presented by [28]. To transform the PDF for the concentrated stress σ_1 curve using Eq. 9, random variable X is the stress concentration factor k, which is uniformly distributed with bounds 50 and 150 and function f(x) is Equation 5, evaluated for t = 100 years according to Eq. 6 and Eq. 7. To transform the PDF for the NCTL ψ_f curve using Eq. 9, random variable X is slope s, which is normally distributed with mean = -0.352 and COV = 20%, and function f(x) is Equation 8 evaluated for t_f = 100 years. Once PDFs are evaluated, the CDFs are computed through summation of $p_\psi(\psi)d\psi$.

In addition to the CDFs, Figure 12 also presents a suggested interpretation of the results as follows. The mean value of ψ_f is greater than 75% of the concentrated stress σ_1 values. Therefore, on average, only 25% of the seam length is expected to crack at 100 years. The 90% exceedance value of ψ_f represents the value at which there is only a 10% chance of having a material with less resistance to cracking. At this value of ψ_f, 92% of the seam length is expected to crack at 100 years.

The flow rate Q through the modeled stress cracks can be computed as [3]:

$$Q = r_0 h_d k_v \left(4 + F\frac{r_0}{D}\right) \quad \text{(Eq. 10)}$$

where r_0 is the radius of the hole or wrinkle beneath the hole, h_d is the hydraulic head at the hole relative to a permeable layer beneath the clay barrier layer, k_v is the vertical hydraulic conductivity, and D is the thickness of the clay barrier layer. F is given by

$$F = 2.455 + 0.685tanh\left(0.6\frac{\ln r_0}{D}\right) \quad \text{(Eq. 11)}$$

Upon inspection of the wrinkles visible in Figure 5, r_0 is conservatively taken equal to 0.15 m. Note that, for this value of r_0, the maximum number of uniformly spaced stress cracks that can uniquely contribute to leakage for a 7m x 7m geomembrane area is 23, corresponding to a hole density of 0.47 holes/m^2 for the overall geomembrane. This value is less than has been assumed in some previous studies (e.g. [6]) for the degraded case. D and k_v depend greatly on the design objectives and regulations for the landfill. For this example, D and k_v are taken as 0.6 m and 1 × 10^{-5} cm/s (1 × 10^{-7} m/s). Given that the final cover is sloped and drained, the

development of head above the geomembrane is unlikely. Therefore, h_d = D = 0.6 m, assuming free drainage below the clay. Substituting into Eq. 11 and Eq. 10, these values yield Q = 4 × 10^{-8} m^3/s for a single hole. Assuming 100% cracking of the seams, this value yields 16 m^3/hectare/day. Note that to achieve this value, a constant supply of water, saturating the upper surface of the clay through the holes, would need to be present continuously. Therefore, this value is extremely conservative compared to water balance models accounting for fluctuations in precipitation.

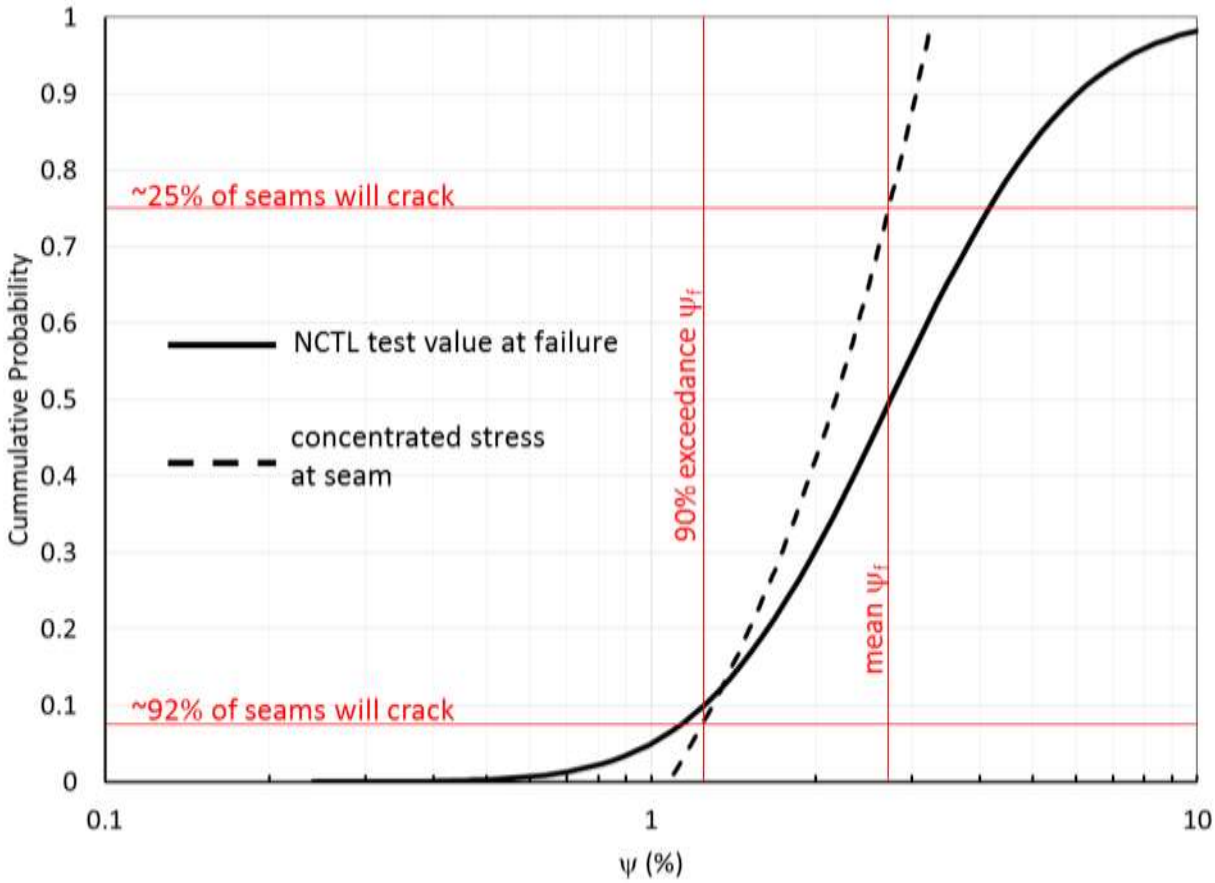

Figure 12. Cumulative Distribution Functions (CDFs) at 100 Years for Comparison of Notched Constant Tensile Load Failure Stress Ratio (ψ_f) with Estimated Concentrated Maximum Tensile Stress (σ_1).

CONCLUSIONS

With CDFs developed according to the above proposed sequence, it is possible to develop a performance assessment model that incorporates material degradation and mechanical site effects into the more general model of system performance. It is anticipated that the point in time t (e.g., 1,000 years after cover construction) for which a particular performance target must be met will be established as part of the regulatory review and performance assessment. Accordingly, for a given PE geomembrane formulation, the degraded tensile properties at time t and the resulting

distribution of cracks will result in a simulation that either meets or does not meet the probabilistic performance targets for the cover system. If the design fails to meet the performance targets due to the degraded condition of the geomembrane, the geomembrane formulation can be re-engineered by selecting different values of geomebrane thickness, antioxidant package, molecular weight, molecular distribution, density, etc. The modeling effect of these improvements will be to develop a revised distribution of crack occurrence at time t reflecting the degraded condition of the revised cover system. If the revised system meets the performance targets, the revised design becomes one of the engineering recommendations for the cover system. According to this methodology, there is a direct connection between the selection of cover system components and the performance assessment, allowing feedback and design optimization, meeting the intent of the engineering/performance assessment interface articulated by [6].

Therefore, for cover system engineering, expert analysis of present and future environmental conditions is needed to select geosynthetics, specify polymer and additive formulations, and configure cover system layering to maximize the effective life of the cover system. Direct accounting for stress crack mechanisms in these assessments will make this process more effective and produce designs that are more reliable. For maximum benefit, the detailed design and performance assessment process must include a directed testing program of candidate PE formulations to determine and adjust basic physical properties and stress crack resistance.

Traditionally, the interpretation of the geosynthetic degradation has been deterministic as opposed to probabilistic. One reason why deterministic analyses are common is the relative scarcity of degradation data and connection of these data with physical phenomena. A methodology to connect these concepts has been presented. Areas for further development of this methodology include: 1) additional studies of stress concentration in geomebranes, 2) improved constitutive models, and 3) procedures for the testing of site-specific PE materials under representative environmental conditions.

Considering that GM manufacturing is performed in lots to support incoming orders and projects, the geosynthetics industry is currently positioned to allow enhanced material specifications to support these proposed design methods. It is important for engineers and analysts alike to be aware of this capability as it can reduce long-term risks at modest cost. The geosynthetic engineering consultants, manufacturers, researchers, testing firms, and installers that comprise the geosynthetic industry are knowledgeable in the materials, methods, and testing protocols required to support the optimization discussed above.

REFERENCES

1. Benson, C. H., Tinjum, J. M., and Hussin, C. J. (1995). "Leakage Rate from Geomembrane Liners Containing Holes." *Geosynthetics '95 Conference Proceedings*. Industrial Fabrics Association International.
2. Giroud, J. P., King, T. D., Sanglerat, T. R., Hadj-Hamou, T., and Khire, M. V. (1997). "Rate of Liquid Migration Through Defects in a Geomembrane Placed on a Semi-Permeable Medium." *Geosynthetics International*. 4(3-4): 349-372.
3. Rowe, R. K. and Booker, J. R. (1998). *Theoretical Solutions for Calculating Leakage through Composite Liner Systems*. Geotechnical Research Centre Report GEOT-18-98. London, Ontario.
4. Schroeder, P. R., Dozier, T.S., Zappi, P. A., McEnroe, B. M., Sjostrom, J. W., and Peyton, R. L., (1994). *The Hydrologic Evaluation of Landfill Performance (HELP) Model: Engineering. Documentation for Version 3*, EPA/600/R-94/168b, September 1994, U.S. Environmental Protection Agency, Washington, DC.
5. Benson, C. H., Albright, W. H., Fratta, D. O., Tinjum, J. M., Kucukkirca, E., Lee, S. H., Scalia, J., Schlicht, P. D., and Wang, X. (2011). *Engineered Covers for Waste Containment: Changes in Engineering Properties and Implications for Long-Term Performance Assessment*, NUREC/CR-7028. U.S. Nuclear Regulatory Commission (NRC), Washington, DC.
6. Ho, C. K., Arnold, B. W., Cochran, J. R., and Taira, R. Y. (2002). *Development of a Risk-Based Probabilistic Performance-Assessment Method for Long-Term Cover Systems,* 2nd ed. SAND2002-3131. Sandia National Laboratories.
7. Hsuan, Y. G., Schroeder, H. F., Rowe, K., Müller, W., Greenwood J., Cazzuffi, D., and Koerner, R. M. (2008). "Long-Term Long-Term Performance and Lifetime Prediction of Geosynthetics." Keynote Paper. *The Fourth European Geosynthetics Conference* (EuroGeo4) Edinburgh, Scotland.
8. Koerner, R. M., Hsuan, Y. G., and Koerner, G. R. (2011). "Geomembrane Lifetime Prediction: Unexposed and Exposed Conditions." GRI White Paper #6. Geosynthetic Institute, Folsom, PA. 27 p.
9. Phifer, M. A. (2012). *Portsmouth On-Site Disposal Cell (OSDC) High Density Polyethylene (HDPE) Geomembrane Longevity*. SRNL-STI-2012-00061. Savannah River National Laboratory.
10. Rowe, R. K. (2005). "Long-Term Performance of Contaminant Barrier Systems." *Géotechnique*. 55(9): 631-678.
11. Rowe, R. K. and Rimal, S. "Aging of HDPE Geomembrane in Three Composite Landfill Liner Configurations." *Journal of Geotechnical and Geoenvironmental Engineering*. 134(7): 906-916.
12. Rowe, R. K. and Sangam, H. P. (2002). "Durability of HDPE Geomembranes." *Geotextiles and Geomembranes*. 20: 77-95.
13. Koerner, R.M. (1998). *Designing with Geosynthetics*, 4th ed. Upper Saddle River, NJ: Prentice Hall.
14. Qian, X., Koerner, R. M., and Gray, D. H. (2002). *Geotechnical Aspects of Landfill Design and Construction*. Prentice Hall, Upper Saddle River, NJ, 717 p.
15. U.S. Nuclear Regulatory Commission (NRC). (2000). *A Performance Assessment Methodology for Low-Level Radioactive Waste Disposal Facilities: Recommendations of NRC's Performance Assessment Working Group*, NUREG-1573. NRC, Washington, DC.

16. Peggs, I. D. (2008). "How long will my liner last?" *Geosynthetics*. Ifai.com. Accessed November 2015.
17. Zhang, J. (2005). *Experimental Study of Stress Cracking in High Density Polyethylene Pipes.* Ph.D. Dissertation. Drexel University.
18. Plastics Pipe Institute. *Handbook of PE Pipe*. Chapter 3 – Material Properties. Plasticpipe.org. accessed October 2015.
19. ASTM International (2012). *Standard Test Method for Evaluation of Stress Crack Resistance of Polyolefin Geomembranes Using Notched Constant Tensile Load Test.* ASTM D5397. West Conshohocken, PA.
20. Koerner, R. M., Hsuan, Y. G., and Lord, A. E. (1992). *Stress Cracking Behavior of HDPE Geomembranes and its Prevention.* Risk Reduction Engineering Laboratory Office of Research and Development, U.S. Environmental Protection Agency. Cincinnati, OH.
21. Nikolov, S., Lebensohn, R. A., and Raabe, D. (2006). "Self-consistent modeling of large plastic deformation, texture and morphology evolution in semi-crystalline polymers." *Journal of the Mechanics and Physics of Solids*. 54: 1350-1375.
22. Geosynthetic Institute. (2015). *Standard Specification for Seam Strength and Related Properties of Thermally Bonded Polyolefin Geomembranes*, GRI Test Method GM19. Geosynthetic Institute, Folsom, PA.
23. Foye, K., Kabalan, Soong, T.-Y., and Koerner, R. M. (2015). "Longevity of Geosynthetic Cover Components." *WM2015* Conference, Phoenix, AZ.
24. Boiko, Y. M., Brostow, W., Goldman, A. Y., and Ramamurthy, A. C. (1995). "Tensile, stress relaxation and dynamic mechanical behavior of polyethylene crystallized from highly deformed melts." *Polymer* 36(7): 1383-1392.
25. Cazenave, J., Sixou, B., and Seguela, R. (2006). "Structural Approaches of Polyethylene Environmental Stress-Crack Resistance." *Oil & Gas Science and Technology*. 61(6): 735-742.
26. Deblieck, A. C., van Beek, D. J. M., Remerie, K., and Ward, I. M. (2011). "Failure mechanisms in polyolefines: The role of crazing, shear yielding and the entanglement network." *Polymer*. 52: 2979-2990.
27. Ang, A. H-S. and Tang, W. H. (1975). *Probability Concepts in Engineering Planning and Design: Volume I-Basic Principles*. John Wiley & Sons. New York, NY.
28. Foye, K. C., Scott, B. and Salgado, R. (2006). "Assessment of Variable Uncertainties for Reliability-Based Design of Foundations." *Journal of Geotechnical and Geoenvironmental Engineering*, ASCE, 132(9): 1197-1207.